Optical-Frequency Magnetic Polarizability in a Layered Semiconductor

Ryan A. DeCrescent,[1,2,*] Rhys M. Kennard,[3] Michael L. Chabinyc,[3] and Jon A. Schuller[2,†]
[1]Department of Physics, University of California Santa Barbara, Santa Barbara, California 93106, USA
[2]Department of Electrical and Computer Engineering, University of California, Santa Barbara, California 93106, USA
[3]Materials Department, University of California Santa Barbara, Santa Barbara, California 93106, USA

(Received 15 June 2021; accepted 28 September 2021; published 20 October 2021)

The optical response of crystals is most commonly attributed to electric dipole interactions between light and matter. Although metamaterials support "artificial" magnetic resonances supported by mesoscale structuring, there are no naturally occurring materials known to exhibit a nonzero optical-frequency magnetic polarizability. Here, we experimentally demonstrate and quantify a naturally occurring nonzero magnetic polarizability in a layered semiconductor system: two-dimensional (Ruddlesden-Popper phase) hybrid organic-inorganic perovskites. These results demonstrate the only known material with an optical-frequency permeability that differs appreciably from vacuum, informing future efforts to find, synthesize, or exploit atomic-scale optical magnetism for novel optical phenomena such as negative index of refraction and electromagnetic cloaking.

DOI: 10.1103/PhysRevLett.127.173604

Introduction.—At optical frequencies, light-matter interactions are dominated by electric dipole (ED) transitions driven by the electric component of the electromagnetic field. The optical-frequency magnetic response is presumed negligible [1]. However, very weak magnetic dipole (MD) transitions play an important role in various atomic and molecular systems [2,3]. For instance, rare-Earth atomic dopants embedded into host crystals exhibit MD photoluminescence [4–6]. Time-reversal symmetry requires these transitions to similarly appear in absorption [7]. Recent work suggests that molecular MD scattering can become as strong as ED scattering through nonlinear magnetoelectric interactions [8,9]. Nonetheless, there are no known materials with an optical-frequency permeability differing from the vacuum value μ_0. This primarily reflects the inherent weakness of MD transitions, which are about 10^5 times smaller than ED transitions in atomic and molecular systems [10]. The combination of small rates, narrow homogeneous linewidths causing poor spectral overlap between distinct dopants [11], and limits on achievable dopant densities precludes the possibility of bulk materials with appreciable deviations from μ_0 at optical frequencies.

A significant linear magnetic response enables unconventional optical phenomena. For example, a simultaneously negative permittivity ϵ and permeability μ enables subdiffraction-limited imaging [12–14]. Electromagnetic cloaking similarly requires an engineered magnetic response [15]. The only known optically magnetic systems are engineered metamaterials [1,14,16]. However, this artificial behavior derives from classical electromagnetic effects in mesoscale resonator structures, not from naturally occurring atomic-scale quantum-mechanical interactions. Generating such phenomena at the atomic scale—such as the recently demonstrated infrared hyperbolic dispersion in *h*-BN [17,18]—provides access to high-quality, deeply subwavelength ($< \lambda/100$) photon modes that cannot be achieved in traditional metamaterials. An atomic-scale resonant optical permeability would challenge existing frameworks for treating bulk light-matter interactions and portend the possibility of realizing bulk materials with novel optical properties.

Two-dimensional (2D) hybrid organic-inorganic perovskites (HOIPs) are self-assembling semiconductor quantum-well systems of tremendous interest for fundamental condensed-matter physics studies [19–25] and optoelectronic applications [26–28]. Recently, fast optical-frequency MD photoluminescence (PL) was identified and quantified in 2D HOIPs [29]. It has been attributed to a self-trapped exciton [24] whose lowest-energy configuration has opposite parity relative to the conventional untrapped ground-state (i.e., 1*s*) exciton [30]. The inferred MD transition rate is approximately 3 orders of magnitude faster than any previously established MD transition [31]. Here, we use a combination of beam engineering and momentum-resolved optical spectroscopy to experimentally demonstrate an appreciable optical-frequency magnetic polarizability in 2D HOIPs.

Results.—Because of their relative weakness, MD transitions are ideally probed in the absence of electric fields. Typical optical beams exhibit both electric and magnetic fields at every position. However, focused azimuthally polarized (ϕ-polarized) beams [Fig. 1(a)] produce "doughnut" patterns with zero electric field intensity ($|\mathbf{E}|^2$) at the focus [32,33] [Fig. 1(b), blue]. The magnetic field intensity ($|\mathbf{B}|^2$) is peaked at the beam focus [Fig. 1(b), orange]. The

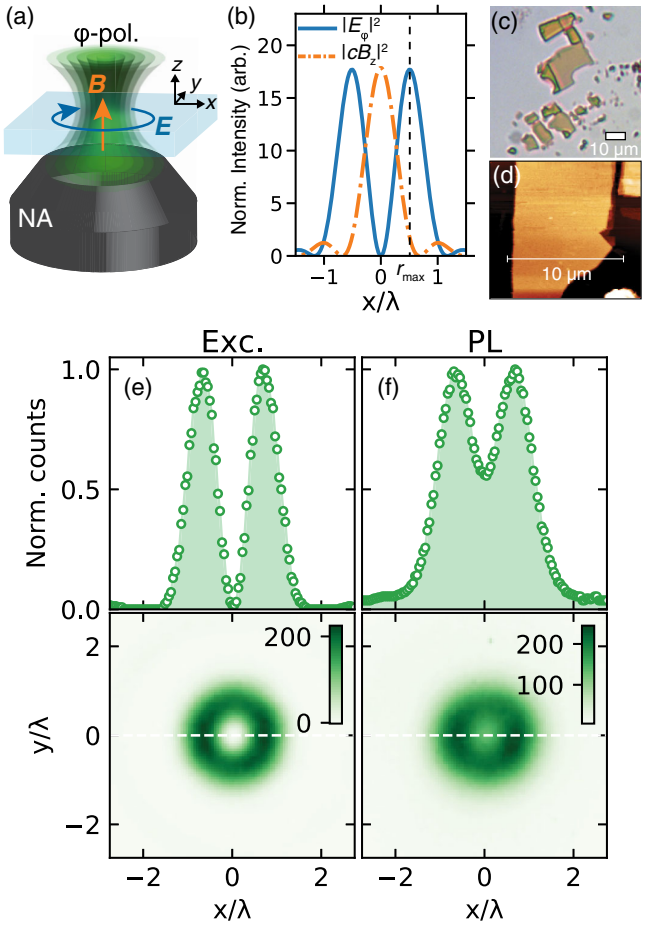

FIG. 1. (a) Schematic of normal-incidence focused ϕ-polarized doughnut beam. (b) Calculated electric ($|\mathbf{E}|^2$, blue solid line) and magnetic field intensities ($|c\mathbf{B}|^2$, orange dot-dashed line) in the beam's focal plane. (c) Optical and (d) atomic force microscope image of 2D HOIP exfoliated flakes. (e) Experimentally measured ϕ-polarized $|\mathbf{E}|^2$ profile of the excitation beam at the substrate surface. (f) PL intensity profile from a 2D HOIP exfoliated flake. Lower panels in (e) and (f) are false-color 2D images (horizontal dashed lines indicate line cuts shown in upper panels).

purely transverse electric field points along the ϕ direction (i.e., in the x-y plane), whereas the magnetic field points in the z direction. An absorbing material in the beam center will be excited only if it responds to the magnetic field.

We produce tightly focused ϕ-polarized beams by passing a linearly polarized TEM_{00} laser through an azimuthal wave retarder, followed by a high-NA oil-immersion objective [Fig. 1(a)] (Supplemental Material Fig. S1 [34]). Experimentally measured electric field intensity profiles for a tightly focused normal-incidence ϕ-polarized beam (wavelength $\lambda = 532$ nm) are shown in Fig. 1(e). The measured electric field intensity is zero at the beam center, maximum at $r_{max} \approx 0.63\lambda$, and shows excellent agreement with calculations (Fig. S1 [34]). A photoluminescent medium absorbs light through ED or MD transitions and subsequently emits light at longer wavelengths. For the samples used here, the beam excites the low-energy tail of a 1s exciton absorption resonance, lying ~360–470 meV below the band gap [20,25]. The absorptance here is small, but probes the sample closer to the MD emission band peak [29]. We use spectral filters to collect PL around 546 nm, close to our 532 nm excitation source, to minimize the effects of chromatic aberration [34]. Spatially resolved PL images reveal the relative absorption of electric and magnetic field components. Previous studies scanned nanoscopic pointlike "probes" to map the ϕ-polarized beam structure [7]. Instead, we use continuous, thin, planar samples and map the entire field structure in a single image. Accordingly, we must account for spatial broadening effects between excitation and PL.

Figure 1(f) shows the PL (bottom panel) from a thin (≈80 nm) exfoliated single-crystal flake of butylammonium lead iodide (BA_2PbI_4). Typical flakes are shown in Figs. 1(c) and 1(d) [34]. The PL generally resembles the excitation spot, but with nonzero intensity at beam center. After accounting for spatial broadening effects, a resolvable portion of the beam-center PL originates from magnetic field absorption.

We quantify the PL broadening with two complementary measurements. First, to avoid potential MD effects, we compare excitation and PL images of BA_2PbI_4 under linearly polarized TEM_{00} Gaussian excitation (Fig. S3 [34]). The PL broadening is accurately reproduced by convolving the excitation profile with a Gaussian point-spread function [34]. This analysis quantitatively accounts for a combination of several possible physical effects, including temporal broadening due to vibrations, light scattering from subwavelength inhomogeneities, PL image aberrations, and exciton spatial diffusion [35]. Images are best fit by a 188 nm Gaussian broadening constant, suggesting that imaging artifacts and aberrations, rather than exciton diffusion (~40 nm), are the dominant source of PL image broadening [35]. Intensity-dependent measurements (Fig. S8) confirm that neither the observed MD absorption, nor the broadening, reflect nonlinear interactions. Measurements were performed at intensities well below the onset of saturation-induced spatial broadening or photodegradation [34].

Second, we compare BA_2PbI_4 PL images to a reference material (Figs. 2 and Supplemental Material Fig. S3 [34])—the semiconducting polymer poly[2-methoxy-5-(2-ethylhexyloxy)-1,4-phenylenevinylene] (MEH-PPV)—with similar absorption and PL spectra [36], optical anisotropies [36], small surface roughness (< 1–2 nm) [37], and short exciton diffusion lengths (~10 nm) [35,38]. Complementary momentum-resolved reflectometry measurements reveal no response to the optical magnetic field (Fig. S2), further validating this choice of reference. PL broadening is accurately reproduced by the same convolution process and parameters despite the different diffusion lengths (Fig. S3).

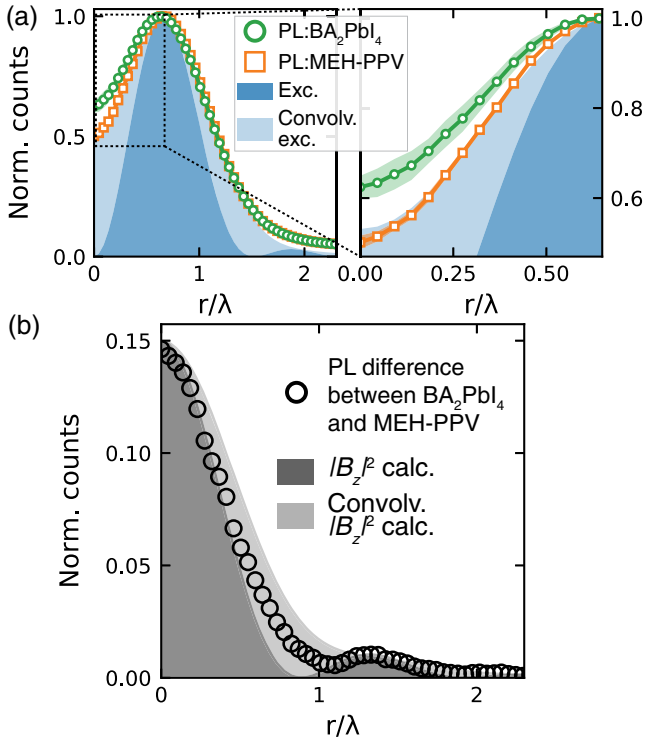

FIG. 2. (a) Comparison of PL from (green circles) BA_2PbI_4 and (orange squares) MEH-PPV under identical ϕ-polarized excitation. Light (dark) blue region: electric field intensity profile with (without) Gaussian broadening. Right: magnified view of the beam center. (b) Black markers: difference between PL profiles from test and reference samples after proper electric field normalization (Fig. S5). Light (dark) gray region: calculated magnetic field intensity with (without) Gaussian broadening.

MEH-PPV PL curves represent our "baseline" ability to resolve the null of a ϕ-polarized excitation beam via PL imaging.

Figure 2(a) shows a direct comparison of BA_2PbI_4 (green circles) and MEH-PPV (orange squares) PL images derived from a measurement and image screening process involving hundreds of measurements on a variety of samples (Supplemental Material Fig. S7 [34]). Open markers (filled regions) represent averages (standard deviations) over all measurements (Fig. S4 [34]). This comparison illustrates a central result of this Letter: *all* ϕ-polarized BA_2PbI_4 PL profiles lie significantly higher than MEH-PPV reference profiles at the beam center (Fig. S4). Excess BA_2PbI_4 optical excitations are generated at the beam center where there is no electric field but a strong out-of-plane magnetic field.

Fitting this PL data to a combination of ED and MD absorption contributions (Fig. S5 [34]), we infer that MD absorption rates (at 532 nm) are 25% of the ED absorption rate. Differences between the two PL curves [Fig. 2(b), black circles) track the calculated out-of-plane magnetic field intensity (gray filled regions)—including secondary lobes at $r/\lambda = 1.25$—remarkably well (Fig. S5). Measured differences between MEH-PPV and BA_2PbI_4 arise from direct absorption of the out-of-plane magnetic field.

To further validate the surprisingly large MD contribution derived above, we independently quantify the linear MD response using momentum-resolved reflectometry (MR) [39]. Momentum-resolved spectroscopies are especially well suited to quantify ED optical anisotropies [39–49] and multipolar light-matter interactions [4–6,29,50] in thin-film systems. Here, for the first time, we resolve a resonant optical-frequency magnetic permeability μ using MR. The imaginary parts of ϵ and μ, respectively, determine the absorption rate of electric and magnetic field components.

Reflectance from a linearly polarized incident plane wave is recorded as a function of its in-plane momentum ($k_\parallel$) and wavelength (λ) by back focal plane imaging [Fig. 3(a)] [34]. Light is incident and collected from the sample substrate using a NA = 1.3 oil-immersion objective. This enables sample excitation well beyond the critical angle of total internal reflection ($k_\parallel > k_0$, where $k_0 = 2\pi/\lambda$ is the light's free-space momentum), where evanescent waves contain large out-of-plane fields. Calculated electric and magnetic field intensities are plotted in Fig. 3(b) for a BA_2PbI_4 thin film illuminated at 532 nm [51]. The p-polarized reflectance in Fig. 3(b) (left panel) is insensitive to the out-of-plane MD response and is thus used to derive in- and out-of-plane permittivities, $\epsilon_\parallel(\lambda)$ and $\epsilon_\perp(\lambda)$ [34]. For s-polarized light (right panel), a large out-of-plane magnetic field develops at large momenta. The s-polarized reflectance is thus most sensitive to the out-of-plane permeability $\mu_\perp(\lambda)$ at large momenta ($k_\parallel > k_0$), where small deviations from $\mu_\perp = 1 + 0i$ produce resolvable differences (~1%–2%) that significantly improve the fit quality [Fig. 3(c)] [34]. Example 533 nm data and fits are shown in Fig. 3(c). (Figure S6 shows data and fits at other wavelengths [34].)

MR results are summarized in Figs. 3(d) and 3(e). The $\epsilon_\parallel(\lambda)$ resonance (blue markers) originates from the $1s$ exciton [19]. The out-of-plane electric permittivity $\epsilon_\perp$ matches the spectral dispersion of $\epsilon_\parallel(\lambda)$ and is associated with a small out-of-plane component of the $1s$ exciton transition dipole moment [47,51,52]. A small but resolvable deviation from $\mu_\perp(\lambda) = 1 + 0i$ (green markers) is observed in both the real and imaginary fit results. Despite significant differences in methodology, the wavelength-dependent ratio $\mathrm{Im}[\mu_\perp(\lambda)]/\mathrm{Im}[\epsilon_\parallel(\lambda)]$ [Fig. 3(f), black curve] agrees remarkably well with the ϕ-polarized beam analysis at 532 nm (black star). The out-of-plane MD absorption observed in ϕ-polarized PL measurements (Fig. 2) produces a nonunity magnetic permeability. This is the only known demonstration of a naturally occurring atomic-scale nonunity optical-frequency magnetic permeability.

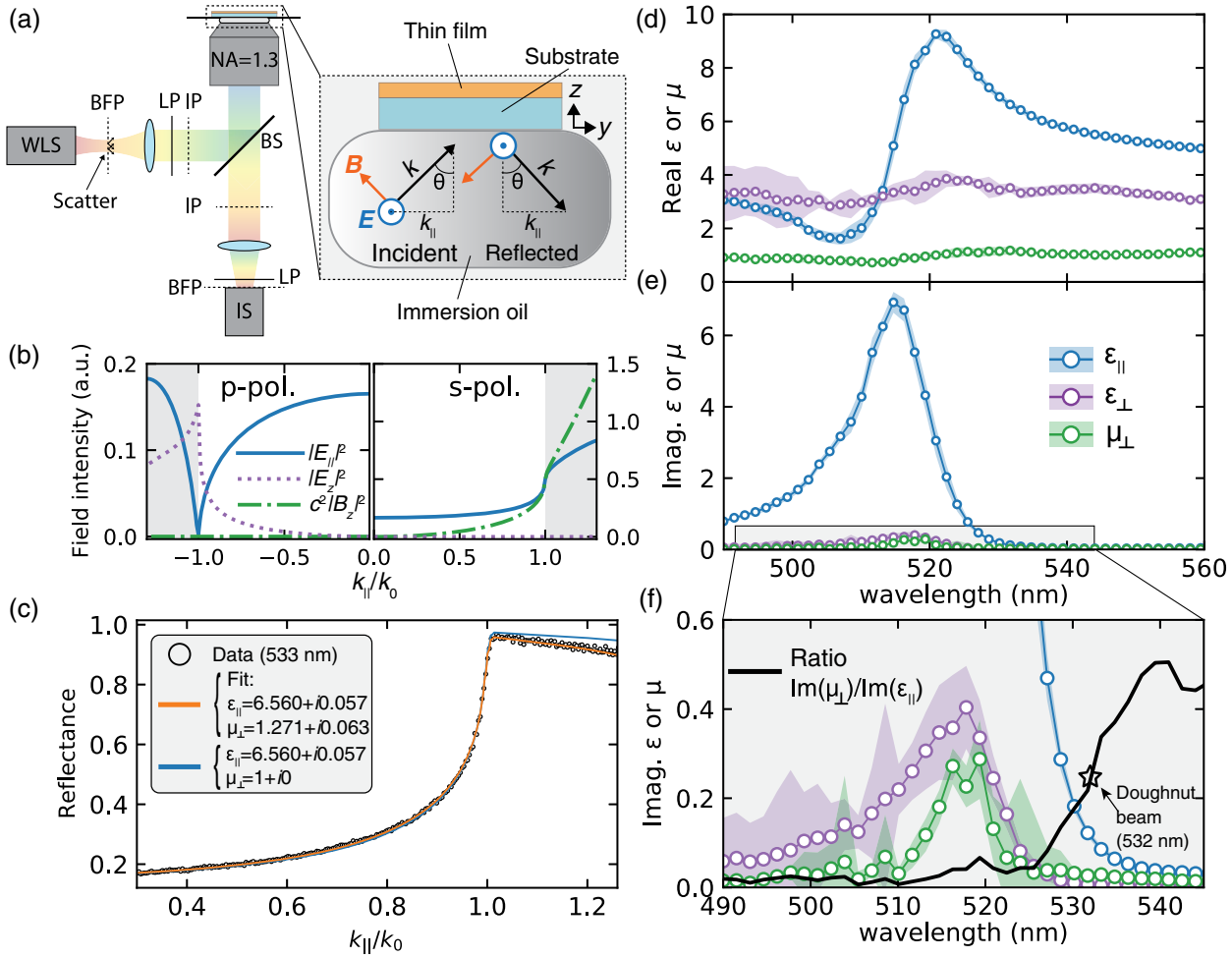

FIG. 3. (a) MR experiment schematic. WLS, white-light source; BFP, back focal plane; IP, real-space image plane; BS, beam splitter; LP, linear polarizer; IS, imaging spectrometer. Blue ellipses represent external Bertrand lenses. Inset shows sample geometry with an s-polarized incident beam. Diffusing film is placed in the BFP nearest the source to scatter light into the system uniformly over momentum space. (b) Calculated field intensities in a 10 nm thin film ($\epsilon_{||} = 6.7 + i0.3$) for (left) p-polarized and (right) s-polarized beams. (c) Single-wavelength (533 nm) s-polarized MR data and fits from a 17 nm 2D HOIP film. (d),(e) Summary of MR results: (d) [(e)] shows the real (imaginary) parts of the complex quantities specified in the legend. (f) Magnified view of (e). Solid black curve, wavelength-dependent ratio $\mathrm{Im}[\mu_\perp(\lambda)]/\mathrm{Im}[\epsilon_{||}(\lambda)]$; black open star marker, value from ϕ-polarized PL excitation measurements. Filled regions correspond to standard deviations over all independent measurements.

The increase in relative MD absorption at longer wavelengths is consistent with redshifted MD PL [29]. Integrated intensities, $f_m = \int \mathrm{Im}[\mu(\lambda)]d\lambda$ and $f_e = \int \mathrm{Im}[\epsilon(\lambda)]d\lambda$, estimate the total magnetic and electric oscillator strengths, respectively. We find $f_m/f_e \approx 0.03$, smaller than values estimated from momentum-resolved PL measurements ($f_m/f_e \approx 0.16$ without thermodynamic corrections) [29]. The quantitative disagreement likely reflects integration over different spectral bands and ensembles of states. In PL measurements, optical excitation is followed by relaxation into the lowest-energy configuration of the exciton-lattice system. In 2D HOIPs, such exciton self-trapping reflects a quasithermal equilibrium that is markedly different from true thermal equilibrium [24,30]. The low-energy MD PL thus appears surprisingly strong, although the intrinsic MD transition rates are relatively small. Although the required initial and final states are always present, thermodynamics dictates that their contributions to PL and absorption spectra will be different. Taking into account the energetic structure [30], we derive a population-corrected intrinsic ratio $f_m/f_e \approx 0.012$ from PL measurements. Remaining quantitative differences between relative rates derived here and from PL likely originate from inaccessible details of the materials energetic structure.

The real and imaginary parts of $\mu(\lambda)$ are intimately related by Kramers-Kronig (KK) relations [53]. Because MR simultaneously provides *unconstrained* estimates for $\mathrm{Re}[\mu(\lambda)]$ [Fig. 3(d)] [39], we can further validate our results by checking for KK consistency. We model the complex

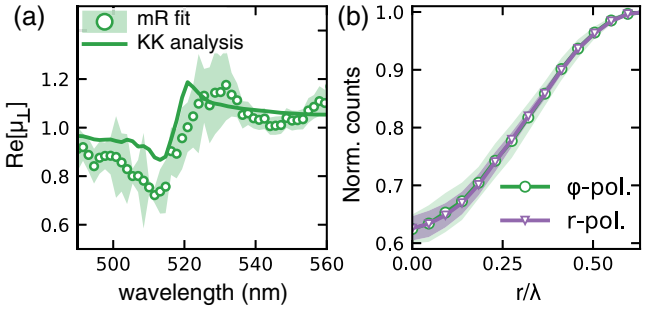

FIG. 4. (a) $\mathrm{Re}[\mu_\perp(\lambda)]$ derived directly from unconstrained MR analysis (markers) and from KK analysis (solid line) of $\mathrm{Im}[\mu_\perp]$. Filled color region: standard deviation over all measurements. (b) Comparison of BA_2PbI_4 PL under tightly focused (purple triangles) r-polarized and (green circles) ϕ-polarized excitation.

permeability using a KK-consistent *ad hoc* superposition of Lorentzian oscillators [54],

$$\mu(E) = \mu_\infty + \sum_{k=1}^{N} \frac{f_k}{E_k^2 - E^2 - iE\gamma_k}, \tag{1}$$

where E is the photon energy and f_k, γ_k, and E_k are the oscillator strength, linewidth, and energy of the kth oscillator. Oscillator energies (E_k) and linewidths (γ_k) are chosen to provide a spectrally smooth response ($\Delta E_k = E_{k+1} - E_k = 1$ meV and $\gamma_k = 5\Delta E_k$) [54]. Oscillator strengths f_k are determined directly from $\mathrm{Im}[\mu_\perp]$ at each spectral position. Finally, $\mu_{\perp,\infty}$ is determined from the real part of the low-energy spectrum. The resulting magnetic polarizability $\mathrm{Re}[\mu_\perp(\lambda)]$ is shown in Fig. 4(a) (solid line). Unconstrained values derived directly from MR (circles) satisfy the KK analysis. At long wavelengths, $\mu_\perp(\lambda)$ asymptotes to $\mu_{\perp,\infty} \approx 1.04$. Near resonance, maximum and minimum values are 1.2 and 0.8, respectively. An equivalent analysis on the in-plane dielectric function $\epsilon_\parallel(\lambda)$ is presented in Fig. S9 [34].

A final qualitative verification of the linear MD absorption can be obtained without a distinct reference material. The 2D HOIPs studied here are known to exhibit an out-of-plane ED response with reports varying between 0.07 and 0.18 of the in-plane ED response [19,47,51]. A radially polarized (r-polarized) doughnut beam exhibits the same intensity profile as the ϕ-polarized beam, but with a strong out-of-plane *electric* field along the beam axis (Fig. S1). The r-polarized beam center should exhibit PL originating from out-of-plane electric field absorption. Spatially resolved PL excitation measurements [Fig. 4(b)], similar to Figs. 1 and 2, reveal similar PL profiles for both r- and ϕ-polarized excitation, both lying well above ϕ-polarized MEH-PPV reference PL profiles.

Conclusions.—The results shown here demonstrate the only known material with "naturally" occurring optical-frequency linear magnetism, indicating that extended crystalline systems may support magnetic permeabilities necessary for achieving optical phenomena previously only seen in inhomogeneous metamaterials. The total variation in μ observed here is relatively modest; a further approximate five- to tenfold increase is needed to reach the μ-near-zero [55] or negative μ values central to metamaterial phenomena. However, the optical response probed here is largely localized in the semiconducting lead iodide layers [19,51], which constitute 46% of the sample's volume. The values of μ derived above thus represent a volumetric average [51]. The intrinsic lead-iodide permeability—which may be similar to 3D HOIPs—is approximately twofold larger (spanning 0.7 and 1.4 with an infrared limit $\mu_{\perp,\infty} \approx 1.08$). Rationally designing materials with a larger response will require further investigation of the physical origins of the MD optical response observed here. We hypothesize that it depends, in large part, on self-trapping effects stemming from exceptionally strong exciton-lattice coupling, as described earlier [24,30]. As such, MD effects may also be prevalent in polaron, edge-state, and white-light emitting light-matter interactions [24]. 2D HOIPs also exhibit strong spin-orbit coupling [21] central to MD transitions in rare-Earth ions [31]. Promising candidates for future investigation include 2D HOIPs where organic components or metal ions (e.g., Sn or Ge) are systematically chosen to tune excitonic parameters related to, e.g., exciton-lattice coupling, dielectric screening, and spin-orbit coupling, interlayer excitons in 2D layered heterojunctions, or distinct quantum-well systems with ED-forbidden band-edge transitions. Finally, we note that the strong MD response shown here suggests a high likelihood for strong MD *nonlinearities* as well, which may generate atomic-scale magnetism at high laser intensities [8]. We anticipate that these results will motivate the reconsideration of assumptions commonly applied in optics and will spur future efforts to synthesize or exploit materials with naturally occurring optical-frequency magnetism deriving from atomic-scale light-matter interactions.

All optical measurement, analysis, theory, and instrument design were supported by the National Science Foundation (DMR-2004093). Sample growth was supported by the U.S. Department of Energy, Office of Science, Basic Energy Sciences, under Award No. DE-SC-0012541.

*Present address: National Institute of Standards and Technology, Boulder, Colorado 80305, USA.
†jonschuller@ece.ucsb.edu

[1] R. Merlin, Proc. Natl. Acad. Sci. U.S.A. **106**, 1693 (2009).
[2] H. Katori, Nat. Photonics **5**, 203 (2011).
[3] M. Germann, X. Tong, and S. Willitsch, Nat. Phys. **10**, 820 (2014).
[4] C. Fattinger and W. Lukosz, J. Lumin. **31–32**, 933 (1984).
[5] N. Noginova, Y. Barnakov, H. Li, and M. A. Noginov, Opt. Express **17**, 10767 (2009).

[6] T. H. Taminiau, S. Karaveli, N. F. van Hulst, and R. Zia, Nat. Commun. **3**, 979 (2012).
[7] M. Kasperczyk, S. Person, D. Ananias, L. D. Carlos, and L. Novotny, Phys. Rev. Lett. **114**, 163903 (2015).
[8] A. A. Fisher, E. F. C. Dreyer, A. Chakrabarty, and S. C. Rand, Opt. Express **24**, 26055 (2016).
[9] A. A. Fisher, E. F. C. Dreyer, A. Chakrabarty, and S. C. Rand, Opt. Express **24**, 26064 (2016).
[10] R. D. Cowan, *The Theory of Atomic Structure and Spectra*, 1st ed., Los Alamos Series in Basic and Applied Sciences (University of California Press, Berkeley, CA, 1981).
[11] T. Bottger, C. W. Thiel, R. L. Cone, and Y. Sun, Phys. Rev. B **79**, 115104 (2009).
[12] V. G. Veselago, Sov. Phys. Usp. **10**, 509 (1968).
[13] J. B. Pendry, Phys. Rev. Lett. **85**, 3966 (2000).
[14] V. M. Shalaev, Nat. Photonics **1**, 41 (2007).
[15] D. Schurig, J. J. Mock, B. J. Justice, S. A. Cummer, J. B. Pendry, A. F. Starr, and D. R. Smith, Science **314**, 977 (2006).
[16] F. Monticone and A. Al, J. Mater. Chem. C **2**, 9059 (2014).
[17] D. N. Basov, M. M. Fogler, and F. J. Garcia de Abajo, Science **354**, aag1992 (2016).
[18] T. Low, A. Chaves, J. D. Caldwell, A. Kumar, N. X. Fang, P. Avouris, T. F. Heinz, F. Guinea, L. Martin-Moreno, and F. Koppens, Nat. Mater. **16**, 182 (2017).
[19] T. Ishihara, J. Takahashi, and T. Goto, Phys. Rev. B **42**, 11099 (1990).
[20] K. Tanaka and T. Kondo, Sci. Technol. Adv. Mater. **4**, 599 (2003).
[21] J. Even, L. Pedesseau, J.-M. Jancu, and C. Katan, J. Phys. Chem. Lett. **4**, 2999 (2013).
[22] C. C. Stoumpos, D. H. Cao, D. J. Clark, J. Young, J. M. Rondinelli, J. I. Jang, J. T. Hupp, and M. G. Kanatzidis, Chem. Mater. **28**, 2852 (2016).
[23] J.-C. Blancon, H. Tsai, W. Nie, C. C. Stoumpos, L. Pedesseau, C. Katan, M. Kepenekian, C. M. M. Soe, K. Appavoo, M. Y. Sfeir, S. Tretiak, P. M. Ajayan, M. G. Kanatzidis, J. Even, J. J. Crochet, and A. D. Mohite, Science **355**, 1288 (2017).
[24] J. Yin, H. Li, D. Cortecchia, C. Soci, and J.-L. Brdas, ACS Energy Lett. **2**, 417 (2017).
[25] J.-C. Blancon, A. V. Stier, H. Tsai, W. Nie, C. C. Stoumpos, B. Traor, L. Pedesseau, M. Kepenekian, F. Katsutani, G. T. Noe, J. Kono, S. Tretiak, S. A. Crooker, C. Katan, M. G. Kanatzidis, J. J. Crochet, J. Even, and A. D. Mohite, Nat. Commun. **9**, 2254 (2018).
[26] H. Tsai, Nature (London) **536**, 312 (2016).
[27] Z. Wang, Q. Lin, F. P. Chmiel, N. Sakai, L. M. Herz, and H. J. Snaith, Nat. Energy **2**, 17135 (2017).
[28] Y. Fu, H. Zhu, J. Chen, M. P. Hautzinger, X.-Y. Zhu, and S. Jin, Nat. Rev. Mater. **4**, 169 (2019).
[29] R. A. DeCrescent, N. R. Venkatesan, C. J. Dahlman, R. M. Kennard, X. Zhang, W. Li, X. Du, M. L. Chabinyc, R. Zia, and J. A. Schuller, Sci. Adv. **6**, eaay4900 (2020).
[30] R. A. DeCrescent, X. Du, R. M. Kennard, N. R. Venkatesan, C. J. Dahlman, M. L. Chabinyc, and J. A. Schuller, ACS Nano **14**, 8958 (2020).
[31] C. M. Dodson and R. Zia, Phys. Rev. B **86**, 125102 (2012).
[32] L. Novotny and B. Hecht, *Principles of Nano-Optics*, 2nd ed. (Cambridge University Press, Cambridge, England, 2012).
[33] K. S. Youngworth and T. G. Brown, Opt. Express **7**, 77 (2000).
[34] See Supplemental Material at http://link.aps.org/supplemental/10.1103/PhysRevLett.127.173604 for experimental and analytical methods and supplemental figures.
[35] M. Seitz, A. J. Magdaleno, N. Alczar-Cano, M. Melndez, T. J. Lubbers, S. W. Walraven, S. Pakdel, E. Prada, R. Delgado-Buscalioni, and F. Prins, Nat. Commun. **11**, 2035 (2020).
[36] M. Tammer and A. P. Monkman, Adv. Mater. **14**, 210 (2002).
[37] M. Liu, Y. Liu, Z. Peng, C. Yang, Q. Mu, Z. Cao, J. Ma, and L. Xuan, Materials **10**, 706 (2017).
[38] A. J. Lewis, A. Ruseckas, O. P. M. Gaudin, G. R. Webster, P. L. Burn, and I. D. W. Samuel, Org. Electron. **7**, 452 (2006).
[39] R. A. DeCrescent, S. J. Brown, R. A. Schlitz, M. L. Chabinyc, and J. A. Schuller, Opt. Express **24**, 28842 (2016).
[40] W. Lukosz and R. E. Kunz, J. Opt. Soc. Am. **67**, 1615 (1977).
[41] W. Brütting, J. Frischeisen, T. D. Schmidt, B. J. Scholz, and C. Mayr, Phys. Status Solidi **210**, 44 (2013).
[42] J. A. Schuller, S. Karaveli, T. Schiros, K. He, S. Yang, I. Kymissis, J. Shan, and R. Zia, Nat. Nanotechnol. **8**, 271 (2013).
[43] S. J. Brown, R. A. Schlitz, M. L. Chabinyc, and J. A. Schuller, Phys. Rev. B **94**, 165105 (2016).
[44] H. Budde, N. Coca-Lpez, X. Shi, R. Ciesielski, A. Lombardo, D. Yoon, A. C. Ferrari, and A. Hartschuh, ACS Nano **10**, 1756 (2016).
[45] Y. Gao, M. C. Weidman, and W. A. Tisdale, Nano Lett. **17**, 3837 (2017).
[46] R. Scott, J. Heckmann, A. V. Prudnikau, A. Antanovich, A. Mikhailov, N. Owschimikow, M. Artemyev, J. I. Climente, U. Woggon, N. B. Grosse, and A. W. Achtstein, Nat. Nanotechnol. **12**, 1155 (2017).
[47] A. Fieramosca, L. De Marco, M. Passoni, L. Polimeno, A. Rizzo, B. L. T. Rosa, G. Cruciani, L. Dominici, M. De Giorgi, G. Gigli, L. C. Andreani, D. Gerace, D. Ballarini, and D. Sanvitto, ACS Photonics **5**, 4179 (2018).
[48] J. Gu, X. Liu, E.-c. Lin, Y.-H. Lee, S. R. Forrest, and V. M. Menon, ACS Photonics **5**, 100 (2018).
[49] M. Brotons-Gisbert, R. Proux, R. Picard, D. Andres-Penares, A. Branny, A. Molina-Snchez, J. F. Snchez-Royo, and B. D. Gerardot, Nat. Commun. **10**, 3913 (2019).
[50] D. Li, M. Jiang, S. Cueff, C. M. Dodson, S. Karaveli, and R. Zia, Phys. Rev. B **89**, 161409(R) (2014).
[51] R. A. DeCrescent, N. R. Venkatesan, C. J. Dahlman, R. M. Kennard, M. L. Chabinyc, and J. A. Schuller, ACS Nano **13**, 10745 (2019).
[52] T. Ishihara, J. Takahashi, and T. Goto, Solid State Commun. **69**, 933 (1989).
[53] A. B. Kuzmenko, Rev. Sci. Instrum. **76**, 083108 (2005).
[54] Y. Li, A. Chernikov, X. Zhang, A. Rigosi, H. M. Hill, A. M. van der Zande, D. A. Chenet, E.-M. Shih, J. Hone, and T. F. Heinz, Phys. Rev. B **90**, 205422 (2014).
[55] A. M. Mahmoud and N. Engheta, Nat. Commun. **5**, 5638 (2014).